ADVANCED HEALTHCARE MATERIALS
www.advhealthmat.de

Chondro-Inductive b-TPUe-Based Functionalized Scaffolds for Application in Cartilage Tissue Engineering

Daniel Martínez-Moreno, Desiré Venegas-Bustos, Guillermo Rus, Patricia Gálvez-Martín, Gema Jiménez, and Juan Antonio Marchal**

Osteoarthritis is a disease with a great socioeconomic impact and mainly affects articular cartilage, a tissue with reduced self-healing capacity. In this work, 3D printed 1,4 butanediol thermoplastic polyurethane (b-TPUe) scaffolds are functionalized and infrapatellar mesenchymal stem cells are used as the cellular source. Since b-TPUe is a biomaterial with mechanical properties similar to cartilage, but it does not provide the desired environment for cell adhesion, scaffolds are functionalized with two methods, one based on collagen type I and the other in 1-pyrenebutiric acid (PBA) as principal components. Alamar Blue and confocal assays display that PBA functionalized scaffolds support higher cell adhesion and proliferation for the first 21 days. However, collagen type I functionalization induces higher proliferation rates and similar cell viability than the PBA method. Further, both functionalization methods induce extracellular matrix synthesis, and the presence of chondrogenic markers (Sox9, Col2a, and Acan). Finally, SEM images probe that functionalized 3D printed scaffolds present much better cell/biomaterial interactions than controls and confirm early chondrogenesis. These results indicate that the two methods of functionalization in the highly hydrophobic b-TPUe enhance the cell-biomaterial interactions and the improvement in the chondro-inductive properties, which have great potential for application in cartilage tissue engineering.

1. Introduction

Regenerative medicine (RM) persecutes the total or partial regeneration of human cells, organs, or tissues to restore or establish normal function.[1] On the other hand, tissue engineering (TE) is a branch of RM based on three pillars: cells, biomaterials, and bioactive molecules.[2] Osteoarthritis (OA), an irreversible and multifactorial disease, is among the different pathologies that can benefit from the RM. The low rate of regeneration in OA is a consequence of the cartilage characteristics, which is an avascular tissue, not lymphatic, and without nerve endings.[3] OA leads to pain and loss of joint function due to articular cartilage loss.[4] It is one of the most common joint disorders resulting from a combination of risk factors, where age and obesity are the most prominent, concerning most frequently in the knees.[5] To current knowledge, there is no OA treatment for stopping or slowing its progression; surgical alternatives are the treatment of choice.[6]

In the last decades, several TE cartilage products like the matrix-associated

D. Martínez-Moreno, D. Venegas-Bustos, G. Rus, G. Jiménez, J. A. Marchal
Instituto de Investigación Biosanitaria de Granada (ibs.GRANADA)
University Hospitals of Granada-University of Granada
Granada E-18071, Spain
E-mail: gemajg@ugr.es; jmarchal@ugr.es
D. Martínez-Moreno, G. Jiménez, J. A. Marchal
Biopathology and Regenerative Medicine Institute (IBIMER)
Centre for Biomedical Research
University of Granada
Granada E-18100, Spain

The ORCID identification number(s) for the author(s) of this article can be found under https://doi.org/10.1002/adhm.202200251

DOI: 10.1002/adhm.202200251

D. Martínez-Moreno, G. Jiménez, J. A. Marchal
Department of Human Anatomy and Embryology
Faculty of Medicine
University of Granada
Granada E-18016, Spain
D. Martínez-Moreno, G. Rus, G. Jiménez, J. A. Marchal
Excellence Research Unit "Modeling Nature" (MNat)
University of Granada
Granada E-18016, Spain
D. Martínez-Moreno, G. Jiménez, J. A. Marchal
BioFab i3D- Biofabrication and 3D (bio)printing laboratory
University of Granada
Granada E-18100, Spain
G. Rus
Department of Structural Mechanics
University of Granada
Politécnico de Fuentenueva
Granada E-18071, Spain
P. Gálvez-Martín
Department of Pharmacy and Pharmaceutical Technology
Faculty of Pharmacy
University of Granada
Granada E-18071, Spain

autologous chondrocyte implantation (MACI), Hyalograft C, NeoCart, NOVOCART 3D, Cartipatch, etc. have tried to mimic articular cartilage.[7] However, most of these therapies involve fibrocartilage formation. To improve the efficacy of such TE procedures, novel approaches, like 3D biofabrication, are in development to introduce stem cells, to avoid the drawback of autologous chondrocytes therapies, into a 3D matrix and culture them in vitro for longer periods, 4–6 weeks.[7] The 3D matrices are known as scaffolds, components that serve as 3D structures to temporarily support autologous cells until they synthesize their matrix components.[8] This fact allows creating a relatively mature tissue in vitro before implantation, with biochemical integrity similar to healthy articular cartilage, since the presence of matrix around the cells is known to enhance donor cell retention,[9] and protect cells from inflammatory agents.[10] Also, scaffolds meet certain requirements such as i) the presence of an adequate surface (roughness and hydrophilicity) to improve cell adhesion, ii) an internal structure (porosity, pore size and structure, and fiber diameter) that supports cellular adherence, proliferation, and differentiation, as well as diffusion of nutrients, oxygen, and wastes, iii) and also possess mechanical and biochemical properties similar to target tissue.[11] Scaffolds can be manufactured with biomaterials, materials intended to interact with biological systems to evaluate, treat, increase, or replace tissues, organs, or functions of the body.

A considerable problem related to the biomaterials is how hydrophobicity and lack of biological recognition sites on the surface of the material provide an unfriendly environment for cell adhesion.[12] To improve cell adhesion, previous functionalization studies focalized on modifying biomaterial surfaces have been developed. Further, surface modifications play a role in cell migration, proliferation, and differentiation of stem cells.[13] Therefore, cell adhesion enhancement would improve cell-biomaterial interaction.[14] Several functionalization methods were used based on the interaction of different components with cell membrane proteins. For example, the surface can be functionalized with the peptide RGD (Arg-Gly-Asp),[15] with 1-pyrene butyric acid (PBA),[16] or with different components present in the extracellular matrix (ECM) like fibronectin or collagen.[17]

Synthetic polyesters, like 1,4 butanediol thermoplastic polyurethane (b-TPUe), have received considerable attention for cartilage TE, due to their appropriate mechanical properties such as the highly elastic recovery capacity.[18] However, its hydrophobicity does not provide the desired environment for cell adhesion and proliferation. Hence, the aim of this study was the set-up of two different functionalization methods, based on the biomaterial coating with collagen type I and PBA, probing how it is possible to reduce the hydrophobicity of b-TPUe improving cell-biomaterial interaction. Two methods were selected due following the objective of comparing a traditional coating method (Collagen type I) adapted from literature[17] with a new methodology (PBA) with reduced costs and good results obtained from making graphene biosensors.[16] Both methodologies are compared by evaluating the efficacy of functionalization by atomic force microscope (AFM) and ninhydrin reagent.

Then, the biological efficacy of both functionalization methods was analyzed by seeding mesenchymal stem cells obtained from Hoffa's fat pad (infrapatellar mesenchymal stem cells (IPFP-MSCs) and performing the subsequent metabolic activity and viability studies. Together with cellular studies, extracellular matrix (ECM) secretion was analyzed through PCR, Glucosamine Glycans (GAG) quantification, and, finally, by SEM, to verify the chondrogenic potential of both functionalized methods.

2. Results

2.1. Characterization and Verification of Functionalization Protocols on b-TPUe

Functionalization methods involve some aggressive reagents, so it is necessary to evaluate their effect on the biomaterial. The surface topology of b-TPUe scaffolds was investigated using a magnifying glass and atomic force microscope (AFM),[19] to probe any macrostructure and/or microstructure surface variation of the fibers derivate by functionalization processes.

For this purpose, b-TPUe scaffolds were immersed in different solutions for 24 h: MilliQ water (**Figure 1**A), which establishes the control; 70% ethanol (Figure 1B) used in the sterilization of the scaffolds; isopropanol used in the 1,6-hexanediamine (Figure 1C) solution involved in the first step of PBA functionalization; and, finally, 0.6 M monopotassium buffer at pH 7.4, where glutaraldehyde (Figure 1D) was dissolved, a fundamental step in functionalization with collagen type I. AFM showed no perceptible surface modification in the monopotassium buffer; however, effects produced by etOH 70% and isopropanol increased rugosity but no degradation appeared (variation less than 100 nm as can be seen in the legend bars of Figure 1B,C).[20] In addition, Figure S1, Supporting Information shows no significant difference in applying 100% etOH or 70% etOH.

Scaffolds already functionalized with collagen (Figure 1E) and PBA (Figure 1F) were analyzed under AFM to compute the presence of any surface modification. Figure 1E probed how collagen fibers were aligned surrounding the scaffold's filaments adding rod-likely patterns of 150 nm in diameter. Figure 1F confirmed the presence of external material attached to the b-TPUe surface. In this case, PBA formed small mountains or 200–400 nm in height. In addition, the power spectra density (PSD) was performed by AFM to compute quantitively any possible exchange in surface patterns.[21] Figure 1G shows buffers effects over scaffolds versus control, whereas, Figure 1H compares functionalized scaffolds concerning control. Here, it is interesting to remark that the glutaraldehyde buffer does not modify the rugosity of scaffold fibers. In contrast, EtOH 70% and 2-prop buffers showed an increase in height of rugosity, manifested at frequencies lesser than 1 micron. Following previous consideration, collagen functionalization increased the height of rugosity at frequencies higher than 1 micron, inducing those collagen fibers to be distributed over scaffold surface letting less than 1 micron between each fiber. Further, when PSD curves from PBA functionalization buffer and 2-prop buffer are compared, they show similar tendencies, showing that there is no major microstructure alteration of the scaffold beyond due to PBA tht the appearance of 400 nm peaks that were not seen with 2-prop buffer.

Surface roughness was evaluated at the macroscopic level through images taken with the Leica Si9 magnifying glass but no differences were found (**Figure 2**A). Comparing these pictures with previous results, it can be estimated that any variation

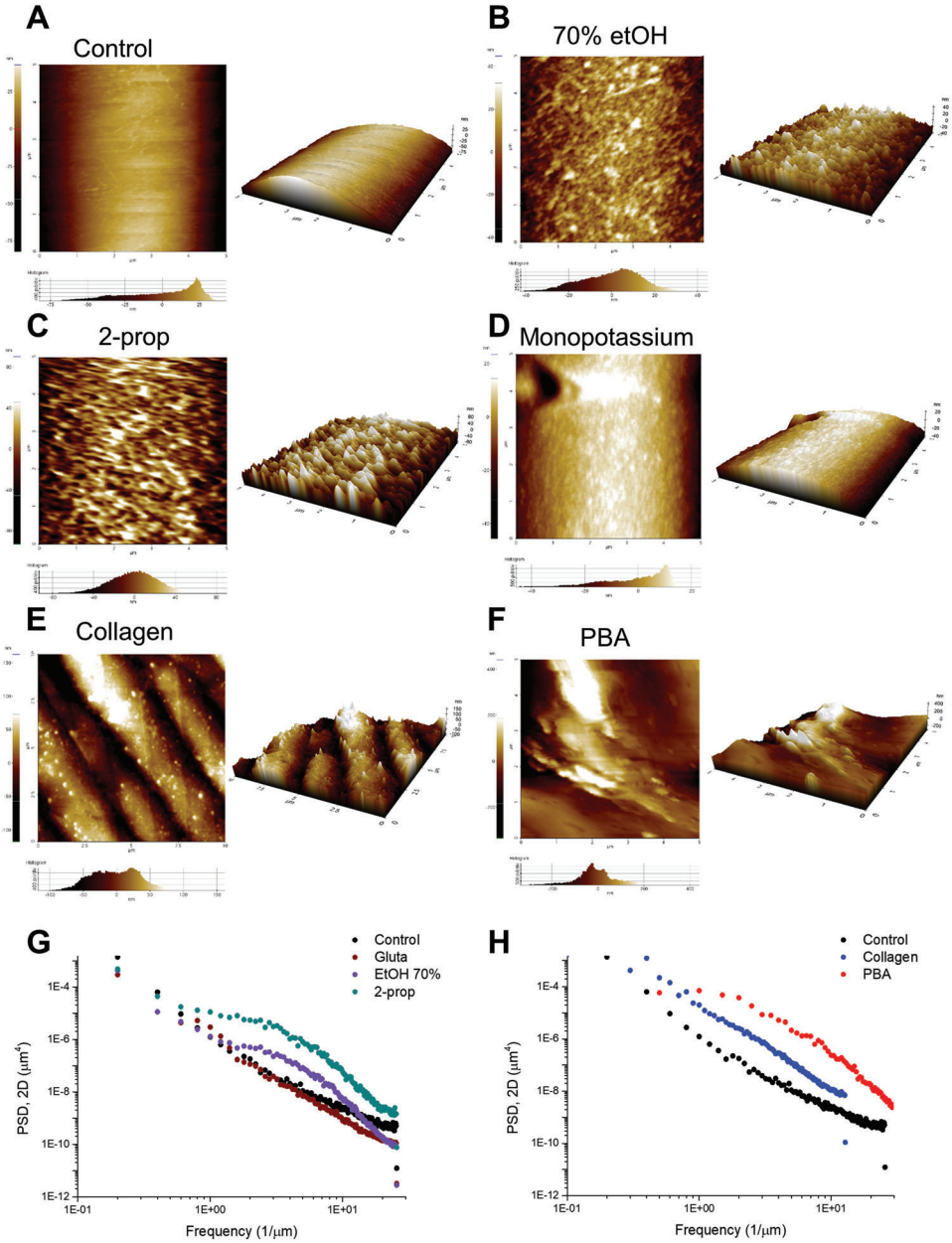

Figure 1. AFM topography analyses. Height images captured from AFM for, A) Mili Q water as control, B) ethanol 70% (mixed with Mili Q water), used to sterilize scaffolds, C) 2-propanol 100% buffer, used to diluted hexamethylenediamine (necessary to PBA functionalization), and D) KH_2PO_4 0.16% Glutaraldehyde buffer used to crosslink collagen fibers in the collagen type I functionalization. E) Height images for collagen functionalized scaffolds, whereas (F) exposes a PBA functionalized fiber. In all cases, the ROI was 5 × 5 µm. G) PSD curves from AFM buffer analyses compared with control. H) PSD of functionalized scaffolds versus control.

perceived by AFM does not modify scaffold microstructure or fiber integrity. In 70% EtOH and 2-prop buffers, it can be distinguished some brighter points for control and glutaraldehyde buffer, which is explained by curves from Figure 1G. In addition, it can be appreciated the size of such points are higher in 2-prop than 70% EtOH as the PSD shows (Figure 2G).

Regarding verification of functionalization protocols, together with AFM (Figure 1E,F), immunofluorescence assays were performed to check the final result. Since the PBA functionalization method consists of two steps, amination process, and PBA addition, to prove that it is possible the binding PBA, it is necessary to check the previous amination of the scaffolds (see Section 1.2, Supporting Information.).

As can be seen in Figure 2B, the ninhydrin standard curve follows a dose-response trend, with the following equation:[20]

$$y = \frac{A1 + (A2 - A1)}{1 + 10^{(\log x0 - x)\cdot p}} \left(R^2 = 0988\right) \quad (1)$$

where: $A1 = 2626$; $A2 = 100\,640$; $\log x0 = 34\,587$

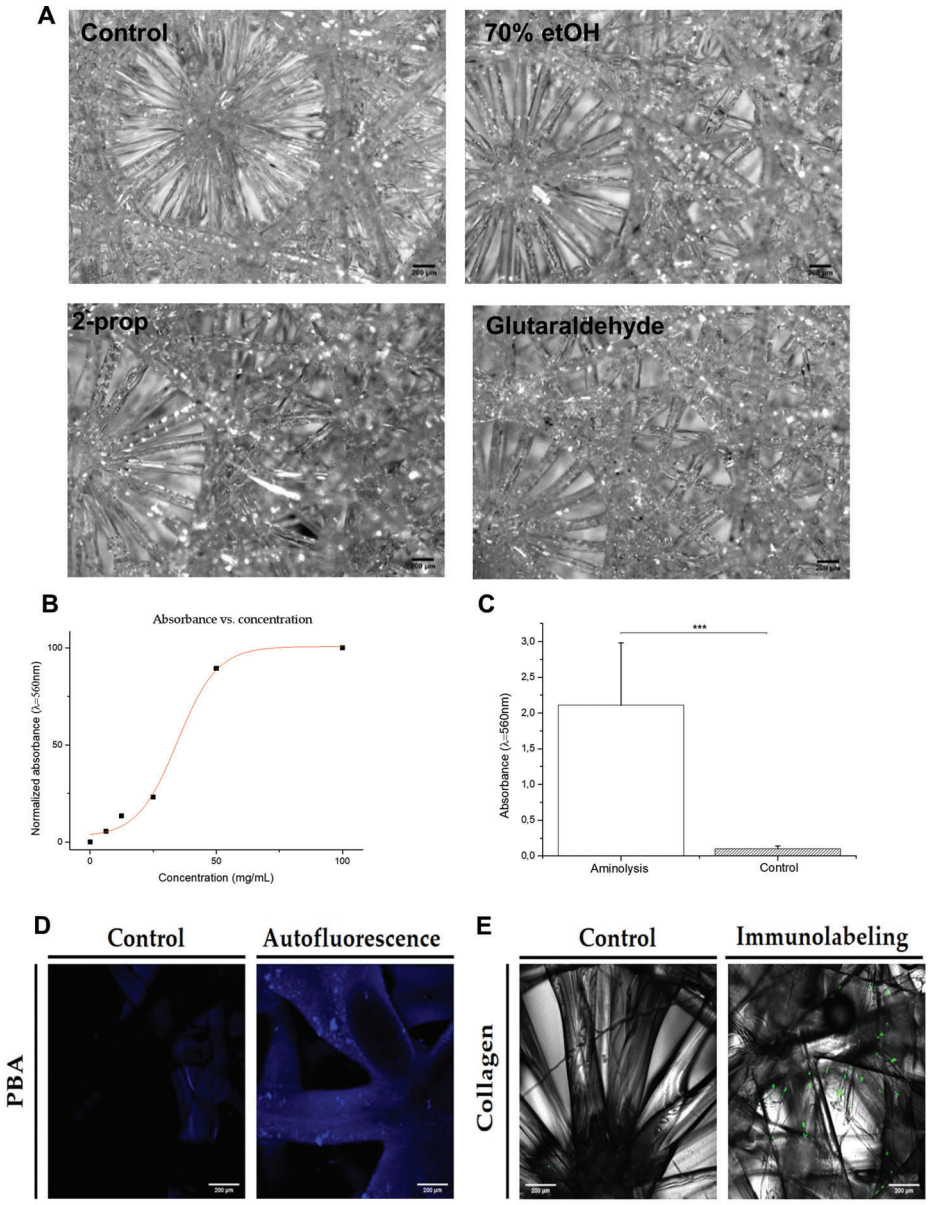

Figure 2. Macroscopic and microscopic characterization. A) Images captured by magnifying glass under transmitted light from different buffers. Control was Mili Q water, 70% ethanol mixed with Mili Q water, pure isopropanol, and KH_2PO_4 0.16% Glutaraldehyde buffer. B) Ninhydrin standard absorbance curve is done by a spectrophotometer. C) Ninhydrin assay for aminated scaffolds (scaffolds embedded inside hexamethylenediamine 2-prop buffer) and control (naïve scaffolds). D) Confocal images from autofluorescence of bTPUe scaffolds functionalized with PBA, and control (non-functionalized). E) Confocal images from immunohistochemistry scaffolds, Immunolabeling as collagen type I functionalization, and control as naïve scaffolds. Magnifying was 10×.

This trend corresponds to the sigmoid model or the Hill model,[21] one of the two commonly used pharmacokinetic models to correlate the pharmacological response with drug concentrations. This model follows the following equation:

$$E = \frac{E_{\max} \cdot C^{\gamma}}{CE_{50}^{\gamma} + C^{\gamma}} \quad (2)$$

where E_{max} would be the V_{max}, CE_{50} the Km, corresponding to the Michaelis–Menten equation, and γ a parameter.

b-TPUe scaffolds treated with 1,6-hexanediamine through the addition of ninhydrin, showed an average absorbance significantly increased ($p < 0.001$) compared with non-aminated scaffolds, allowing to verify that the amination process was efficient (Figure 2C). To finalize with PBA, Figure 2D displays the autofluorescence of b-TPUe without functionalization and after PBA treatment, and it can be distinguished the mountain patterns shown in the AFM as brighter fluorescence points.

Also, an immunofluorescence assay was performed to visualize the components of the functionalization.

Immunofluorescence in Figure 2E to check collagen type I presence (in green), shows the previous homogeneity distribution with no difference between fluorescence points, and the collagen can be appreciated over fibers at different focal planes indicating that collagen functionalization was produced on the whole scaffold.

In conclusion, results showed differences in the roughness of the material depending on the condition to which they were subjected, but no apparent degradation was observed and, more importantly, it can be established that functionalization succeeded in both cases.

2.2. Evaluation of Cell Metabolic Activity and Cell Viability in PBA and Collagen Type I Functionalized-Scaffolds

Functionalization processes aim to improve the superficial properties of b-TPUe since it is a highly hydrophobic material. The reduction of hydrophobicity and the addition of different components to the surface of the scaffolds can enhance cell-biomaterial interaction and consequently maintain cell viability and increase proliferation rate. For this purpose, IPFP-MSCs were seeded in the functionalized b-TPUe scaffolds and metabolic activity was measured to assess cell attachment and proliferation by using Alamar Blue reagent (**Figure 3**A).

IPFP-MSCs were isolated from osteoarthritic patients and expanded until low passages 3–6. IFPF-MSCs were characterized (Figure S2, Supporting Information) using the guidelines proposed by the International Society for Cellular Therapy (ISCT).[22] After that, IPFP-MSCs (700 000 cells per well) were seeded over scaffolds and incubated for 4 h at 37 °C, then a fresh medium was applied. The progression of metabolic activity was monitored for 21 days for all conditions. In the case of collagen type I, we did additional studies to adjust the concentration of glutaraldehyde (Figure S3, Supporting Information). Results on day 3 confirmed that the optimum concentration of glutaraldehyde for collagen functionalization was 0.16%.

On day 1, the difference in metabolic activity and, therefore, cell proliferation was found between all conditions ($p < 0.001$) (Figure 3A). Both functionalization methods presented higher metabolic activity than controls. Moreover, collagen type I-functionalized scaffolds (0.16% of glutaraldehyde) showed higher metabolic activity than PBA-functionalized scaffolds with a high statistically significant difference ($p < 0.001$). On day 3, metabolic activity increased in control and PBA-functionalized scaffolds while it was maintained in collagen type I-functionalized scaffolds ($p < 0.05$) (Figure 3A). Although on day 3, control showed an increase in its alamar blue reduction, the metabolic levels dropped again and they remained the rest of the days (Figure 3A). On day 7, metabolic activity increased in collagen type I-functionalized scaffolds while PBA-functionalized was preserved ($p < 0.05$). Even so, both functionalization methods continued to show a higher metabolic activity compared to the control. In contrast, on days 14 and 21 the decreasing trend continued in collagen type I-functionalized scaffolds, whereas the PBA method expressed maintenance (day 14) or increase (day 21) of proliferation compared with both, collagen functionalization and control ($p < 0.001$).

Further, to clarify if metabolic responses were in concordance with cellular content in the scaffolds, Alamar Blue reduction fold increase curve was plotted (Figure S3A, Supporting Information) and DNA fold increase curve was obtained (Figure S3B, Supporting Information). The metabolic ratio (over DNA content) from Alamar Blue reduction versus DNA fold increase[23] for functionalized scaffolds shows a correlation between the increase of metabolic activity and DNA content, where PBA functionalized scaffolds presented a higher ratio compared with collagen type I functionalized scaffolds at day 21 (Figure 3B).

On the other hand, images obtained from the b-TPUe scaffold samples under different conditions using confocal microscopy corroborated the results obtained with the Alamar Blue assay and Alamabr Blue reduction fold increase/DNA fold increase. The feasibility study was performed on days 1, 7, and 21 after cell seeding (Figure 3C–K). Results were correlated with proliferative assays, with an increase in cell adhesion at day 1 significantly higher in collagen type I scaffolds (Figure 3E) than control (Figure 3C) and PBA functionalization (Figure 3D). It can be appreciated that cells were found included in the regions between fibers, something that does not happen in other cases. Also, on day 7, viability continued to keep in both functionalized scaffolds (Figure 3G,H) and, even more, cell proliferation allowed those cells to colonize the entire surface of the fibers. On the contrary, the control (Figure 3F) did not present living cells in the majority of scaffold surfaces. Finally, on day 21 (Figure 3I–K), the viability was preserved with very poor viability on control. In contrast, the cell distribution over PBA functionalized and Collagen type I functionalized scaffolds was slightly different, whereas in the PBA case cells surrounded fibers, in Collagen type I seems to grow forming clusters.

2.3. Evaluation of the Chondrogenic Potential of Functionalized Scaffolds

Considering the results from metabolic assays and cell viability, we evaluated if cells were producing a chondrogenic matrix. Consequently, GAG quantification versus DNA concentration was calculated (**Figure 4**A–C), and gene expression by PCR was carried out (Figure 4D).

For GAG quantification, scaffolds were seeded over 21 days inside a common cell medium. GAG determination showed significant differences between functionalized samples and controls (Figure 4A, $p < 0.001$). Although control scaffolds presented a similar number of cell content (Figure 4B), no GAG content was extracted from these scaffolds. After 21 days, although GAG concentration decreased for both functionalization methods, they exhibit higher results in comparison to control. Moreover, PBA functionalized scaffolds displayed a significant increase in GAG content than collagen type I functionalized scaffolds. Using another standard protocol for DNA extraction (papain buffer solution assay) showed that in collagen type I functionalization method there was a significant reduction of DNA content from day 1 to day 21; however, in PBA functionalization no difference was founded along time (Figure 4B), which is in concordance with Figure S3B, Supporting Information. Moreover, collagen type I functionalized scaffolds had higher DNA concentrations on both days ($p < 0.001$). DNA content

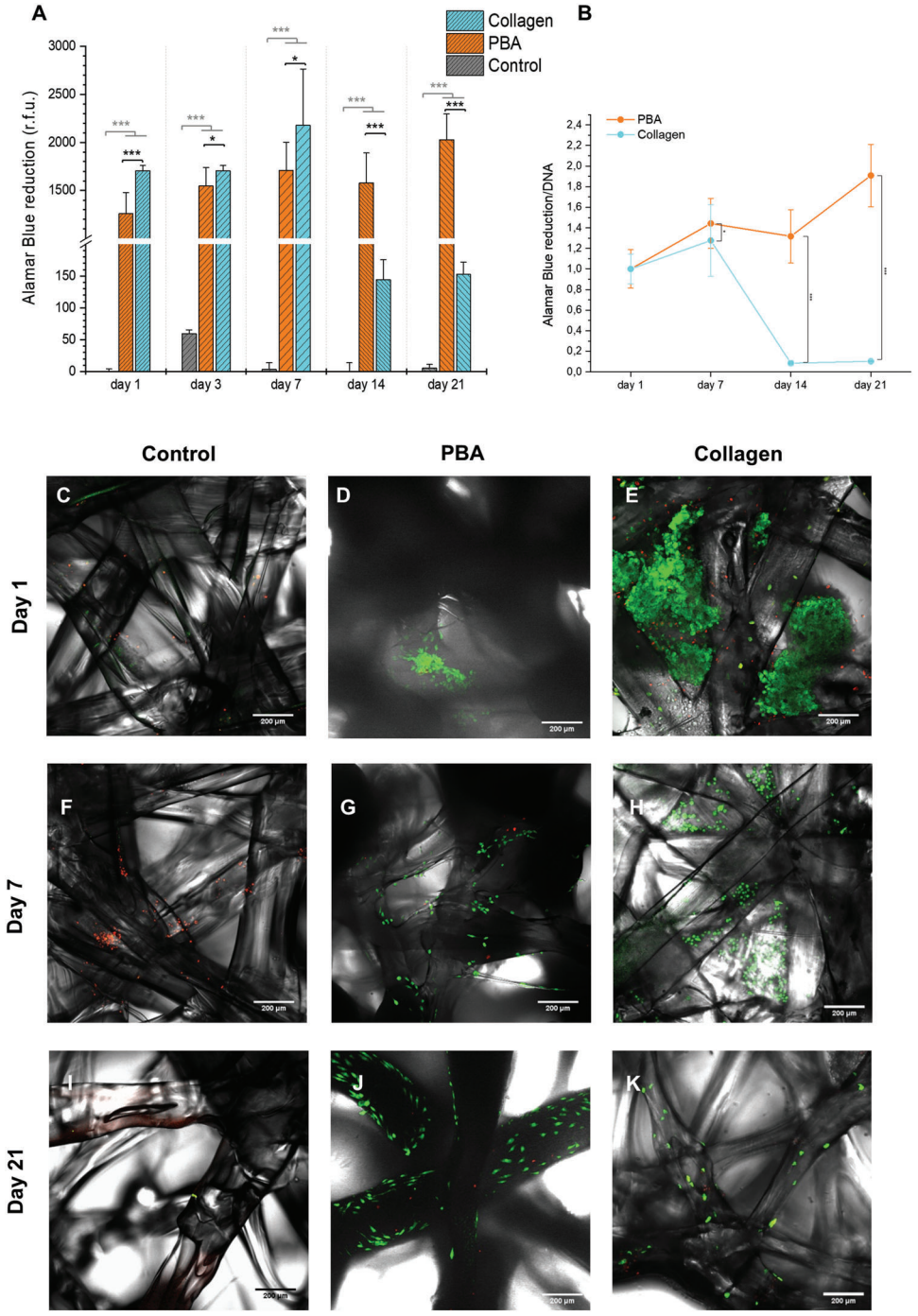

Figure 3. Metabolic and cell proliferation of bTPUe functionalized scaffold loaded with IPFP-MSCs. A) Alamar Blue reduction fluorescence response (λ = 570 nm) for bTPUe scaffolds without treatment (control), PBA functionalized scaffolds, and Collagen type I functionalized scaffolds at days 1, 3, 7, 14, and, 21. B) Alamar Blue reduction/DNA fold increase (obtained by dividing Figure S4A, Supporting Information by Figure S4B, Supporting Information) curves for PBA functionalized scaffolds and collagen type I functionalized scaffolds along 21 days. ($n = 3$) (***, $p < 0.001$; *, $p < 0.05$; N.S., not significance), C–K) Confocal images from Live/Dead assay (Thermo Fisher Scientific) of naïve bTPUe scaffolds as control and both functionalization protocols. Magnifying was 10×.

from controls was not negligible, but, in any case, it was significantly less than functionalization methods. Additionally, the absence of any GAG on both days declares that cells attached to bare filaments do not produce ECM (PBA, $p < 0.05$; Collagen, $p < 0.001$).

Nevertheless, the representation of ratio between GAG versus DNA concentrations (Figure 4C) showed a significant difference between functionalized scaffolds with control samples ($p < 0.001$). Besides, PBA functionalized scaffolds presented a higher ECM synthesis ratio than collagen type I functionalized scaffolds,

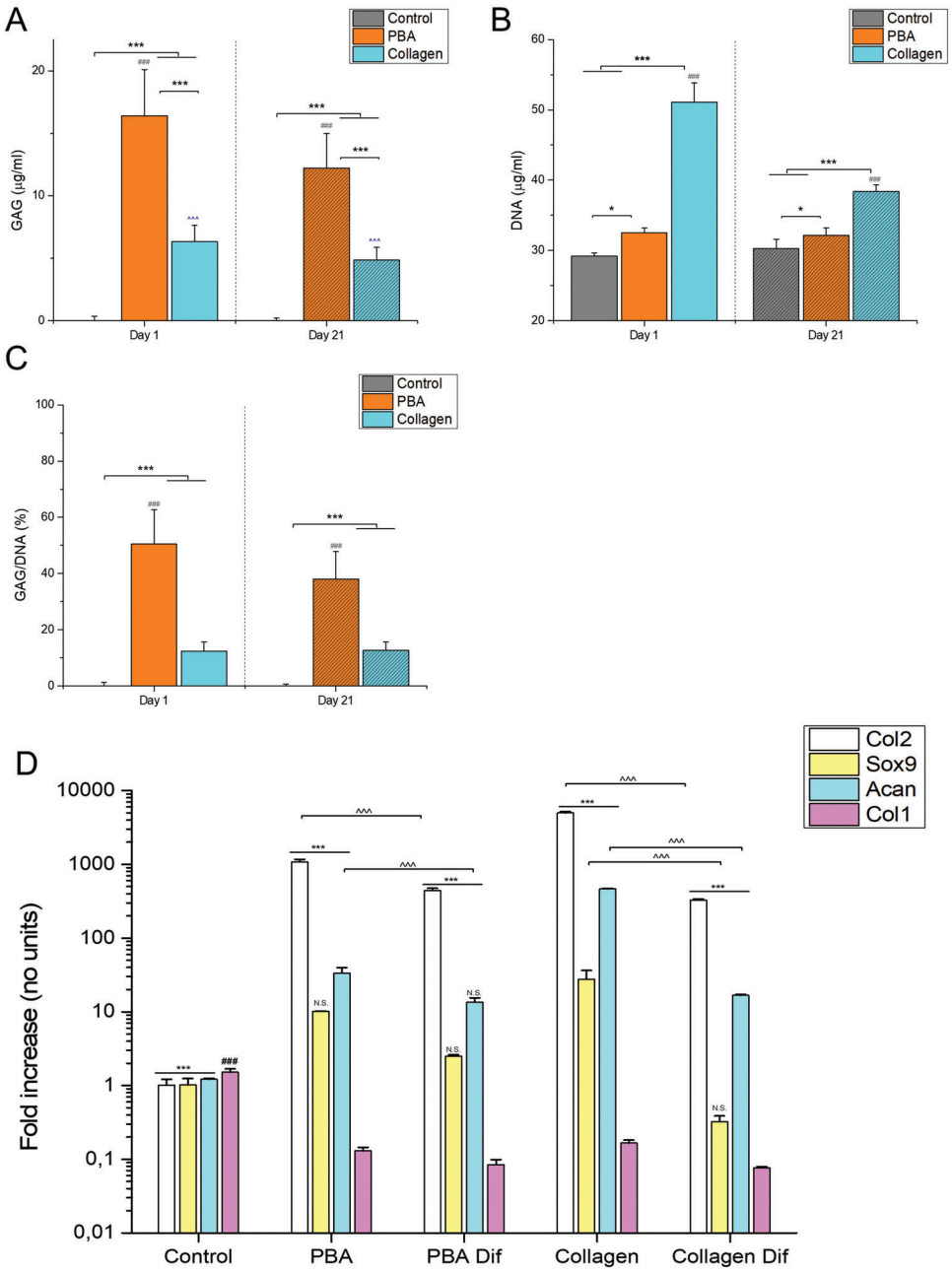

Figure 4. Chondro-inductive properties of bTPUe functionalized scaffold loaded with IPFP-MSCs. A) GAG concentrations obtain through papain assay for naïve bTPUe scaffold and both functionalization protocols on day 1 and day 21. B) DNA concentrations were obtained through papain assay for naïve bTPUe scaffolds and both functionalization protocols on day 1 and day 21. C) GAG/DNA ratios for naïve bTPUe scaffolds and both functionalization protocols on day 1 and day 21 ($n = 3$). (***, $p < 0.001$; *, $p < 0.05$; ###, $p < 0.001$; ^^^, $p < 0.001$). D) Gene expression fold increase obtained through qPCR. Control used were IPFP-MSCs cultured at day 0. PBA was scaffolds functionalized with PBA under normal cell medium, PBA Dif was the same scaffolds under chondrogenic medium, both at day 21. Collagen scaffolds were collagen type I functionalized scaffolds under normal medium, Collagen Dif was same scaffolds under chondrogenic medium, both at day 21. Col2 was COL2A1. Sox9 was the Transcription factor SOX-9. Acan was Aggrecan. Col1 was COL1A1. ($n = 3$) (***, $p < 0.001$; *, $p < 0.05$; ###, $p < 0.001$; ^^^, $p < 0.001$; N.S., not significance). Black bars correlated chondrogenic markers of functionalized scaffolds versus control. N.S: implies exception in previous correlation. Blue # correlates control concerning others. Grey bars correlate PBA with PBA Dif. Green bars correlate Collagen with Collagen Dif.

however, in Collagen type I samples synthesis ratio was preserved along the 21 days, whereas, in PBA protocol that production was reduced ($p < 0.001$).

To explore the chondro-inductive potential, functionalized scaffolds were treated with both chondrogenic and normal mediums for 21 days. Gene expression results (Figure 4D) showed that functionalized scaffolds present higher chondrogenic potential than controls ($p < 0.001$), except for Sox9 in differentiated medium cases and PBA and aggrecan (Acan) in differentiated PBA, where no significant differences were found. Surprisingly,

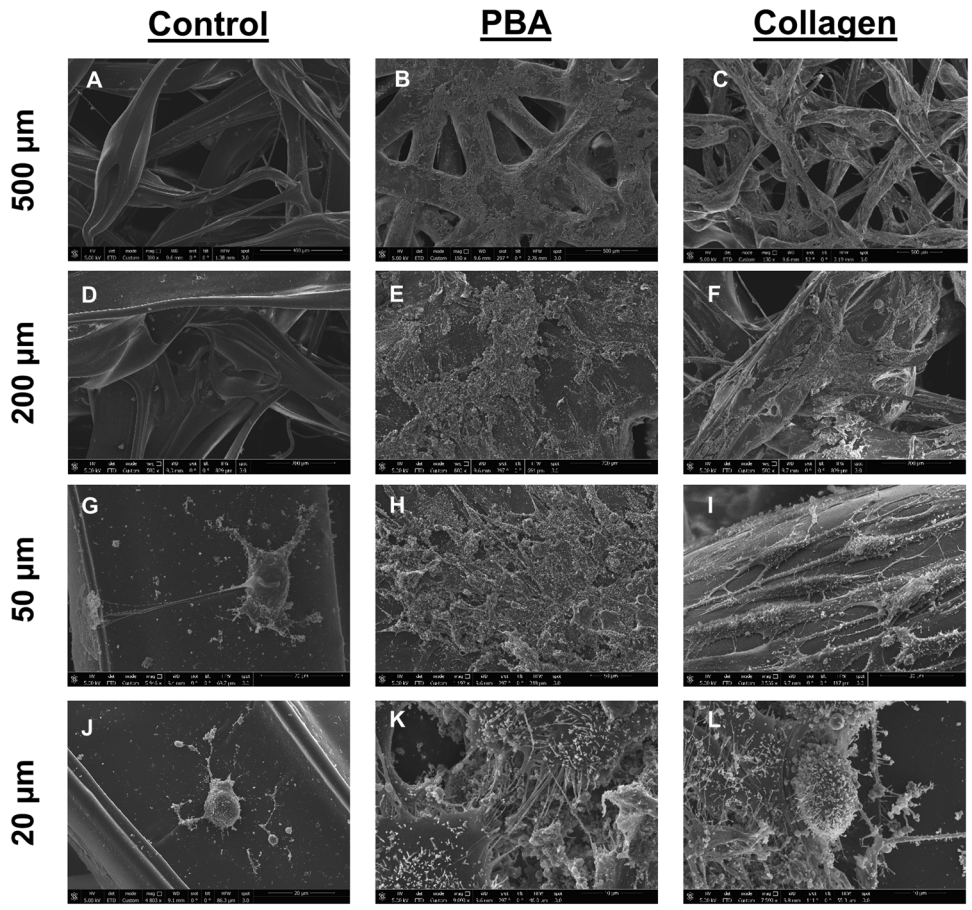

Figure 5. SEM images from control, PBA functionalized and collagen type I functionalized scaffolds on day 21. A–E) Control images, where (B) shows a magnification of a viable cell. (E) shows poor cell-biomaterial interaction. F–J) PBA images, (F) clearly shows the presence of ECM over scaffold fibers, (G) represents cell-cell interactions. (J) shows cell-ECM interactions. Collagen images, where (I) shows the presence of ECM over scaffold surface, (K) shows cell-biomaterial interaction and ECM preserved morphology, and (L) shows a chondrocyte-like cell.

in functionalized scaffolds cultivated with a normal medium the gene expression for collagen type II, Sox9 and Acan were higher than in those cultured in the medium of differentiation, which implies no necessity of using additional growth factors. Collagen type I functionalized scaffolds with normal medium highlighted over rest of cases with almost 10 000 times more collagen type II expression and 1000 times of Acan than control ($p < 0.001$). Even more, collagen type I expression in functionalized scaffolds was significantly lesser than in control (Figure 4D, $p < 0.001$).

Conclusively, GAG/DNA ratios and gene expression assays indicate that, in contrast with control scaffolds, functionalized scaffolds produced more ECM and are chondro-inductive.

2.4. Analysis of Cell Morphology and ECM Appearance by Scanning Electron Microscopy (SEM)

After confirming that functionalized scaffolds showed high cell viability during 21 days and that they were able to produce ECM without any additional growth factor, cell morphology and ECM appearance were evaluated by SEM assays after 21 days (**Figure 5**). Figure 5A,D,G,J represents control scaffolds at different magnifications, where it can perfectly distinguish the presence of living cells attached over the surface of the scaffold, but those cells presented a poor cell/biomaterial interaction (Figure 5G,J). It can be pointed out that, correlatively with ECM expression results, no presence of ECM was found.

In contrast, PBA functionalized scaffolds (Figure 5B,E,H,K) exhibited higher cellular content than control, and there was a high presence of ECM forming a homogeneous surface that covered scaffold fibers. Figure 5K shows how differentiated IPFP-MSCs are interacting between each other and in Figure 5H it is appreciated how cells are immersed in a dense ECM and expanded over it.

Collagen type I scaffolds were by far the ones with a higher number of cells and with the presence of a great amount of ECM (Figure 5C,F,I,H). All the scaffold surfaces were covered by cell content ECM and cells. More interestingly, differentiated IPFP-MSCs produced ECM over angles that formed fiber cross-sections. In Figure 5L it can be found the presence of a cell with a chondrocyte-like appearance with a spherical shape and some cilium embedded in ECM. Moreover, a much natural cell-biomaterial response than other cases was observed with cells growing through naïve scaffolds fibers (Figure 5I).

In summary, SEM assay confirmed all previous results where control scaffolds presented very few cells with apoptotic-like morphology and functionalized methods showed an increased cell number with chondrocyte-like morphology and with a considerable amount of ECM evolving both cells and scaffolds.

3. Discussion

The elasticity and stiffness of the 3D scaffolds are important for the formation of articular cartilage tissue since it is subjected to cyclic mechanical forces due to the corporal movement.[24] The important factors that regulate previous characteristics in scaffolds are the pore size and scaffold fiber geometry. Wang et al.[25] assume that large pore sizes increase ECM production of chondrocytes, a fact that was contrasted by previous literature.[26,27] Similarly, it has been established that a pore size between 370 and 400 μm as the optimum one for chondrogenesis.[28] In this work, we also used a similar pore size (375 μm) that together a high interconnectivity of scaffold fibers along different layers is essential for conditioning cartilage biomechanics and creating an adequate cellular niche for cell differentiation.[29]

The polyurethane (PU) family has been used as a scaffold biomaterial for cartilage TE due to its proper tensile strength, high elasticity, and good biocompatibility.[30–33] It has been previously demonstrated[30] the adequate properties of PU for cartilage substitutes including their viscoelastic behavior[24,30] and the high elastic recovery (> 99% recovery).[33] However, its high hydrophobicity makes it a necessity to adapt its surface to improve cell-matrix interfaces to ensure good cell adhesion and differentiation[34,35] or by specific surface properties including topography,[36] potential, and charge.[37,38]

In the present work, 3D scaffolds were printed with b-TPUe, a thermoplastic PU filament comprising methylene diphenyl diisocyanate (MDI) and 1,4-Butanediol, where PU structure consists of three complex monomers: a macrodiol, a diisocyanate, and a chain extender, based on which several different PU materials can be synthesized.[39] In previous works, we have demonstrated the biocompatibility of b-TPUe[40] and its similar cartilage mechanical behavior.[29] Here, the 3D printed b-TPUe scaffolds were functionalized using two different methodologies based on collagen type I and PBA to improve their biological properties. In each of the functionalization methods, the solutions to which the material was subjected were diverse, and they exert an effect on the microstructure of the b-TPUe scaffolds. At the macroscopic level, no differences were observed on the surface, however, AFM analysis showed differential effects in the roughness of the material. This superficial characteristic was greater when scaffolds were subjected to 70% ethanol and isopropanol. The roughness obtained does not significantly alter its properties because its increase was less than 1 nm. In addition, in previous literature, it has been described that an increase in roughness implies a decrease in hydrophobicity.[19]

Functionalization with components present in the ECM is recurrent and mostly offers good results.[41] The chondrogenesis process begins with MSCs and over time cell proliferation and differentiation toward chondrocytes occur, finally giving rise to hypertrophy and ossification.[42] As differentiation proceeds, a matrix that is rich in fibronectin and collagen type I is replaced with one that contains Collagen type II and aggrecan as the main components.[43] This is why collagen type I was used for functionalization of the 3D printed b-TPUe scaffolds.

Also, functionalization with PBA was performed. Hinnemo et al. reported interesting results using PBA to attach it non-covalently to graphene through π-π stacking, a common approach to non-covalently attaching functional groups.[16] No use of PBA over PU surfaces has been previously published, and the only use of PBA with application in TE was done by Luo et al. in 2015.[44] Its PBA consists of a pyrene group that contains π electrons and a carboxylic group that can be used to facilitate further functionalization. In the present study, b-TPUe has not had a high density of delocalized π-electrons like graphene so it is not possibly established a π-π stacking between b-TPUe and PBA.[16] For this reason, first, it is necessary for the amination process to establish amino groups in the b-TPUe surface and possibly later the interaction between amino groups and PBA by the carboxylic group. Finally, π-π stacking will be able between PBA and aromatic amino acids of membrane cell proteins.

Collagen has been coated successfully onto numerous hydrophilic biomaterials. Due to the hydrophobic characteristic of b-TPUe, the development of a method that reduces its hydrophobicity and allows coating with collagen was necessary. For this reason, collagen type I functionalization was a more complex protocol than PBA and there were several steps involved. First, the use of urea was necessary for the reduction of hydrophobicity through the deposition of polysaccharides and proteins to subsequently achieve the binding of collagen.[45] Collagen type I must be cross-linked to be used as a functional replacement in vivo due to its high degradation rate and low biomechanical strength.[46] This fact was obtained when glutaraldehyde was decreased in the protocol, where the absence of it presented a very poor metabolic cell response. As it is known, glutaraldehyde can become toxic if it is not used in the right concentration and if its unreacted functional groups are not blocked.[47] As a consequence, different concentrations of glutaraldehyde and glycine (a blocking agent) were tested to optimize the accurate concentration that did not compromise cell viability, and, at the same time, the tertiary structure of collagen type I was preserved. An optimal concentration of 0.16% of glutaraldehyde and 0.5 M of glycine were found to ensure cell viability and preservation of collagen tertiary structure.

In the study of the topographic properties of our 3D printed b-TPUe scaffolds, the AFM results showed how PBA increased the global rugosity height, but frequencies observed in the PSD curves were considerably lesser than control and collagen functionalization. Consequently, the heterogeneity of this functionalization method is higher. Contrary, collagen type I fibers had an estimated diameter of 300 nm,[48] therefore, they reached a high level of homogeneity.

Further results showed an increase in cell adhesion in functionalized scaffolds opposite to native scaffolds, implying that our methodology overpasses the first issue of this research.[49] Even, PBA scaffolds increase cell proliferation along 21 days, meanwhile, collagen type I functionalized scaffolds only preserved that proliferation over 7 days to abruptly reduce at days 14 to 21. Moreover, DNA content was measured to verify if changes in cell proliferation were in agreement with cellular metabolism. The ratio between Alamar Blue reduction fold increase and DNA fold increase indicated that in PBA a decrease in cell content was not associated with a decrease in cell metabolism, which suggests that

the increase in metabolism activity is in part due to an increase in ECM synthesis as was found in GAG/DNA ratio and SEM, as previously described.[50]

Thereby, both functionalized methods reached good cell viability values for 21 days with no apparent difference between them, and obtained results were considerably higher than previous works.[29,40] Nevertheless, PBA is an inexpensive reagent and a fast process of functionalization that allows obtaining functionalized b-TPUe in 2 h instead of 3 days, which could be used to manufacture b-TPUe directly coated with PBA.

In addition, it was very surprising to verify that functionalized scaffolds did not need any special medium to induce chondrogenesis. These results were in concordance with literature where Collagen type I induced chondrogenesis,[46] even in the case of PBA scaffolds where this ability has been not probed before. This was confirmed in confocal and SEM assays where living cells were easily founded at the corners formed by fiber's crosslinking between scaffold layers, thus, IPFP-MSCs were more condensed in those regions, a factor that facilitates chondrogenesis.[51] Regarding Col type II and Sox 9 expression, it is interesting to verify how the samples where their production was greater, also presented the higher Acan production.[52] It is known that in healthy cartilage, chondrocytes are constantly remodeling their ECM, and they use their pericellular matrix for such purposes.[52] Our results are in concordance with previous criteria as well as it was obtained before by other researchers in literature.[53] Zhang et al.[54] analyzed the importance of scaffold geometry for enhancing in vivo osteogenesis and chondrogenesis without any additional implementation of cell content before scaffold implantation, and also how additional non-physiological materials as bredigite increased cellular proliferation and ECM synthesis,[55] which is in concordance with our results. The importance of biochemical cues inside in vivo niche and all the proteomic pathways developed by inflammatory processes present in osteoarticular disorder, such as OA are essential for regulating cell proliferation and differentiation.[56] As we discussed in a previous work,[57] at the initial stages of OA, cartilage is trying to remodel with no positive result and the tensile strength is reduced.[58] Applying biomaterials that avoid such biomechanical instability would be highly beneficial for cartilage repair; thereby, a good functionalization method and an adequate geometry should promote chondrogenesis avoiding the use of chondrogenic medium.

Finally, SEM images concordats with all previous results showing a very poor cell-biomaterial interaction and apparently, no cell-cell interactions in non-functionalized scaffolds. Our functionalized methods not only satisfy cellular demand for an adequate attachment but also the cell-cell interactions,[59] a critical factor for adequate biomaterials. In addition, it seems that either PBA as Collagen type I induce chondrogenic differentiation results in concordance with other researches for osteointegration.[59] IPFP-MSCs culture for 21 days changed their characteristic MSC morphology (more elongated and planar) to a spherical conformation embedded in matrix with some cilium[60–62] indicating what seems differentiation into chondrocyte-like morphology.[63] Moreover, it was found how differentiated IPFP-MSCs tented to expand their ECM to the fiber's crosslinking regions, an aspect that has been described before.[29]

4. Conclusions

In this work, we have adapted for the first time, not one, but two different possible methods for bTPUe functionalization in a biomaterial with mechanical properties similar to cartilage[29,30,33,64] but with high hydrophobicity. Both of them presented improved IPFP-MSCs adherence, proliferation, and chondro-inductive properties. Thus, 3D printed b-TPUe scaffolds treated with 1,6-hexanediamine and PBA or with collagen type I showed an improvement in cell-biomaterial interaction with increased cell adhesion and proliferation after 21 days. More importantly, IPFP-MSCs attached to the functionalized scaffold were able to increase the chondrogenic differentiation potential even without additional differentiation medium or other growth factors. In addition, SEM images remarked the wide gap of cell/biomaterial interaction between functionalized scaffolds and not functionalized ones.

Regarding the surface modification motifs, AFM displayed an increase in rugosity of both methods although the patterns were different. SEM images showed how cells adapt better to such patterns and, as consequence, the functionalized scaffolds significantly increased their adhesiveness cell properties.

Although we probed both collagen type I and PBA functionalization methods however, we recommend PBA functionalized procedure due to its reduced cost in terms of reactive prices and time-consuming.

In summary, the improvement in surface properties of 3D printed b-TPUe scaffolds favoring cell-biomaterial interaction and its chondrogenic properties results in a biomaterial with a highly compliant nature and elastic recovery capacity similar to cartilage, which can overcome the limitations of the current scaffold-based approaches. Nonetheless, further in vivo experiments must be done to demonstrate the clinical potential of cartilage TE.

5. Experimental Section

Sample Processing: The IPFP-MSCs were extracted directly from osteoarthritic patients of the Hospital Universitario de Málaga, Spain. Ethical approval for the study was obtained from the Ethics Committee of the Clinical University Hospital of Málaga, Spain (ethic permission number: 02/022010 Hospital Virgen de la Victoria, Málaga). Informed patient consent was obtained for all samples used in this study. Hoffa's fat pad was harvested from the inside of the capsule excluding vascular areas and synovial regions. The isolation and culture protocols of IPFP-MSCs were done according to López-Ruiz et al. [65]. IPFP-MSCs were characterized following the established criteria of the International Society for Cellular Therapy (ISCT) (see Section 1.1, Supporting Information).[22]

Printing of 3D Scaffolds: The design of the desired scaffold was performed using the Cura 3D program, and its printing with the Monoprice Mini V2 bioprinter inside a class II laminar flow cabinet was carried out. The bioprinter was thoroughly cleaned in 70% ethanol and left overnight under UVs.

The scaffolds were designed to fit a multiwell 48-well plate. Therefore, they took cylindrical geometry: diameter of 10 mm, the height of 2 mm; layer height of 200 μm. The extruder's movement speed was set at 14 mm s^{-1} and the working temperature was 230 °C. Finally, the flow rate (the speed at which the filament travels through the extruder) was determined at 1 mm s^{-1}.

To ensure the complete sterility of the scaffolds, they were placed in a Petri dish and were washed with 20%, 50%, and 70% ethanol. After wash-

ing, UV radiation was applied for 1 h on both sides. A new wash with 1% PBS of antibiotic (P/S) was carried out to remove the ethanol that may remain. Finally, the b-TPUe scaffolds were immersed in PBS 1% antibiotic, and they were incubated until functionalization protocols.

Functionalization with PBA: Scaffolds were placed in a multi-well plate and immersed in a 10% isopropanol solution of 1,6-hexanediamine for 30 min at room temperature for the PBA functionalization method. After, scaffolds were rinsed in 1-pyrene-butyric acid (PBA; Sigma Aldrich) at 5 mM DMSO (Sigma Aldrich). Finally, several washes were done with PBS.[1,2]

Functionalization with Collagen Type I: Scaffolds were immersed in urea (Sigma Aldrich) for 24 h at room temperature.[17] Subsequently, the collagen type I of calfskin (0.1% in 0.1 M Acetic Acid) (Sigma Aldrich) was added overnight. After, 0.625% glutaraldehyde in 0.6 M monopotassium buffer at pH 7.4[17] was used in the first functionalization processes. Then, a second functionalization protocol was tested, to improve cell adhesion. For this purpose, glutaraldehyde concentration was reduced from 0.625% to 0.16% and used in the same buffer. This reduction of glutaraldehyde was done to ensure cellular viability.[66] Finally, to block the unreacted functional groups of glutaraldehyde, 0.2 M and 0.5 M glycine was added for 10 min, respectively for each of the glutaraldehyde pumps.

Magnifying Glass and Atomic Force Microscope (AFM): For surface identification of modified samples, they were studied before (control) and after surface modification at a macroscopic and microscopic level. Samples were introduced in different solutions for 24 h: MilliQ water (control); 70% and 100% ethanol; in isopropanol and 0.6 M monopotassium buffer at pH 7.4. For this study, samples were cleaned before being used. Leica Si9 magnifying glass was used for macroscopically studying the surface properties of scaffolds in different conditions. At the microscopic level, AFM NX20 analyses were performed without additional pretreatment.

Immunofluorescence of Collagen Type I and PBA after Functionalization Process: To probe collagen type I presence in b-TPUe biomaterial surface after functionalization method, indirect immunofluorescent visualization of collagen type I was performed. Collagen-functionalized scaffolds were treated with a primary antibody against collagen type I (Sigma Aldrich) and a secondary antibody (Thermofischer). PBA possesses autofluorescence, so no staining was necessary, and scaffolds were observed before and after the functionalization process ($\lambda ex = 340$ nm and $\lambda em = 405$ nm). Images were obtained using a confocal microscope (Nikon Eclipse Ti) and analyzed with Image J software (v. 1.52i, USA).

Seeding of the Scaffolds with Cells: IPFP-MSCs suspension (7×10^5 cells) were pipetted onto each scaffold and incubated for 4 h at 37 °C to allow cell attachment. The cell-seeded scaffolds were transferred into new low attachment 48-well culture plates with 1 mL of medium. All samples were incubated under a 5% CO_2 atmosphere at 37 °C for 21 days. The culture medium was replaced every 2 days.

Metabolic Activity: The metabolic rate was assessed by colorimetric Alamar Blue assay (Thermo Fisher Scientific) following the manufacturer's instructions on days 1, 3, 7, 14, and 21 days after seeding. Cell-free 3D scaffolds were used as controls, and data were normalized to the appropriate control. The fluorescence intensity was measured using a plate reader (Synergy HT, BIO-TEK).

In addition, DNA was also determined on days 1, 7, 14, and 21 in collagen and PBA samples to check the difference in adhesion and alamar blue reduction among functionalization protocols. To do this, DNA content was also approximated with DAPI, but the extraction protocol was different: samples were inserted in different Eppendorf tubes, and 1 mL of distilled water was added to induce osmotic lysis at 37 °C for 1 h. Immediately after, the tubes were transferred to −80 °C for 1 h. This protocol was adapted from the one proposed by Sika et al.[67] and it was not used for estimating DNA concentration.

Cell Viability: The Live/Dead assay (Thermo Fisher Scientific) was used following the manufacturer's instructions to evaluate the viability of IPFP-MSCs previous to and after the bioprinting process on days 1, 7, and 21. The scaffolds were observed using a confocal microscope (Nikon Eclipse Ti) for visualization and image. Images were analyzed with Image J software (v. 1.52i, USA).

DNA and GAG quantification: Scaffolds ($n = 3$) were digested with papain (25 uL mL^{-1} in FBE) after 1 day and 21 days in culture with DMEM Glutamax (Thermo) 1% P/S, 10% FBS. GAG quantification was approached using dimethyl methylene blue (DMMB) colorimetric assay, whereas DNA content was estimated using a fluorometric marker (DAPI staining). The standard curve for the GAG protocol was used using a gradient curve of Chondroitin sulfate (Sigma) and the DNA standard curve was done using DNA from Calf Thymus (Sigma Aldrich).

Cartilage Gene Expression: To determine the cartilage gene expression, RNAs for collagen type II, aggrecan, and collagen type I (as a control) were analyzed using PCR assays. Primer sequences were used as in previous works.[68]

Scaffolds were cultivated for 21 days with an initial cell concentration of 2×10^6 cells per scaffold. Both functionalized cases were studied under normal medium (DMEM, 10% FBS and 1%P/S) and chondrogenic medium (DMEM 1%PS, 1% ascorbic acid, 1% proline, 1% insulin transferrin serum-ITS, 1% of transforming growth factor-beta 3, TGFB3, and 0.1% dexamethasone). After, total messenger RNA (mRNA) from attached IPFP-MSCs was extracted using 1 mL RNAzol RT (Sigma) per Eppendorf/scaffold ($n = 3$) on day 21. Then, mRNA was reverse transcribed into cDNA using the Reverse Transcription System kit (Promega) following the manufacturer's protocols. Finally, a quantitative real-time polymerase chain reaction (qRT-PCR) was executed using an SYBR green master mix (Promega) under the company's instructions. Gene expression levels were normalized to the housekeeping gene glyceraldehyde 3-phosphate dehydrogenase (GADPH) and showed a fold change relative to the value of control IPFP-MSCs at day 0.

Scanning Electron Microscopy: The scaffolds were imaged with an FEI Quanta 400 microscope (Thermo Fisher Scientific-FEI, Fremont, CA, USA) with an Everhart-Thornley detector (E-TD) for dry and conductive samples in high vacuum mode. Samples were incubated for 21 days (2×10^6 cells per scaffold), and, then, they were fixated with 2% glutaraldehyde overnight at room temperature. The next day, they were rinsed in 0.1 M cacodylate buffer and saved at 4 °C. Then, samples were prepared for SEM following standard protocols: i) several washed with PBS, ii) dehydration series with ethanol (30–100%), iii) they were critically point dried in an Emscope CPD 750, iv) mounted on aluminum SEM stubs, and v) sputter coating with a conductive material (gold-palladium alloy, Sputter Coater 108 Auto).

Statistical Analysis: Under each condition, three experiments were performed to assess variability ($n = 3$, data representation corresponds to mean ± SD). The data were processed and represented using the software Origin 9.0 (OriginLab Corporation, Northampton, MA, USA). Homoscedasticity was verified on all data (Shapiro-Wilk). The Student's two-tailed t-test was applied to analyze the data with a confidence interval of 0.05. If any, outliers were neglected with the IQR (interquartile range) procedure, where multiple samples were compared by the ANOVA test, and means were compared employing a two-tailed Bonferroni Test with a confidence interval of 0.05. In figures, p-values < 0.001 are represented with "***," < 0.01 "**," and, < 0.05 "*."

Supporting Information

Supporting Information is available from the Wiley Online Library or from the author.

Acknowledgements

The authors gratefully thank Ana Santos, Mohamed Tassi, Fátima Linares, Isabel Sánchez, and Gustavo Ortiz from the C.I.C. (University of Granada) for the excellent technical assistance. This research was supported by the Ministerio de Economía, Industria y Competitividad (ERDF funds, project RTC-2016-5451-1), the Fundación Mutua Madrileña (project FMM-AP17196-2019), the Consejería de Economía, Conocimiento, Empresas y Universidad de la Junta de Andalucía (ERDF funds, projects B-CTS-230-UGR18, PY18-2470, SOMM17-6109, and P18-FR-2465), and the Instituto de Salud Carlos III, ERDF funds (DTS19/00145). Ministry of Education grant numbers EQC2018-004508-P, DPI2017-83859-R, and UNGR15-

CE-3664 and Junta de Andalucía grant numbers B-TEP-026-UGR18, IE2017-5537, P18-RT-1653.

Conflict of Interest

The authors declare no conflict of interest.

Author Contributions

D.M.-M., G.J., and J.A.M. contributed to the conception and design. D.M.-M. and D.V.-B. collected and/or assembled the data. D.M.-M., G.R., and P.G.-M. contributed to data analysis and interpretation. D.M.-M. and D.V.-B. wrote the manuscript. D.M.-M., G.J., and J.A.M. revised the manuscript.

Data Availability Statement

Data sharing is not applicable to this article as no new data were created or analyzed in this study.

Keywords

1-pyrenebutyric acid, bioprinting, collagen type I, functionalization, osteoarthritis, scaffolds

Received: January 29, 2022
Revised: May 13, 2022
Published online: July 29, 2022

[1] C. Mason, P. Dunnill, *Regener. Med.* **2007**, *3*, 1.
[2] R. Langer, J. P. Vacanti, C. A. Vacanti, A. Atala, L. E. Freed, G. Vunjak-Novakovic, *Tissue Eng.* **1995**, *1*, 151.
[3] X. Houard, M. B. Goldring, F. Berenbaum, *Curr. Rheumatol. Rep.* **2013**, *15*, 375.
[4] D. Heinegård, T. Saxne, *Nat. Rev. Rheumatol.* **2011**, *7*, 50.
[5] S. Chen, P. Fu, H. Wu, M. Pei, S. Chen, P. Fu, H. Wu, M. Pei, *Cell Tissue Res.* **2017**, *370*, 53.
[6] R. Martínez, C. Martínez, R. Calvo, R. Martínez Figueroa, C. Martínez Figueroa, R. Calvo Rodriguez, D. Figueroa Poblete, *Rev. Chil. de Ortop. y Traumatol.* **2015**, *56*, 45.
[7] E. A. Makris, A. H. Gomoll, K. N. Malizos, J. C. Hu, K. A. Athanasiou, *Nat. Rev. Rheumatol.* **2015**, *11*, 21.
[8] M. Tatsumura, M. Sakane, N. Ochiai, S. Mizuno, *Cells Tissues Organs* **2013**, *198*, 405.
[9] A. Tseng, I. Pomerantseva, M. J. Cronce, A. M. Kimura, C. M. Neville, M. A. Randolph, J. P. Vacanti, C. A. Sundback, *Cartilage* **2014**, *5*, 241.
[10] S. R. Sampat, G. D. O'connell, J. V. Fong, E. Alegre-Aguarón, G. A. Ateshian, C. T. Hung, *Tissue Eng., Part A* **2011**, *17*, 2259.
[11] M. R. Rad, M. J. Eghbal, N. Nadjmi, A. Khojasteh, S. R. Motamedian, M. Jafari, Z. Paknejad, *J. Biomed. Mater. Res., Part B* **2015**, *105*, 431.
[12] W.-B. Tsai, C.-H. Chen, J-Fu Chen, K.-Y. Chang, *J. Mater. Sci.: Mater. Med.* **2006**, *17*, 337.
[13] S. Metwally, U. Stachewicz, *Mater. Sci. Eng., C* **2019**, *104*, 109883.
[14] J. A. Sanz-Herrera, E. Reina-Romo, *Int. J. Mol. Sci.* **2011**, *12*, 8217.
[15] H. Zhang, S. Hollister, *J. Biomater. Sci., Polym. Ed.* **2009**, *20*, 1975.
[16] M. Hinnemo, J. Zhao, P. Ahlberg, C. Hägglund, V. Djurberg, R. H. Scheicher, S.-L. Zhang, Z.-B. Zhang, *Langmuir* **2017**, *33*, 3588.
[17] T. Douglas, H. J. Haugen, *J. Mater. Sci.: Mater. Med.* **2008**, *19*, 2713.
[18] A. Haryńska, I. Gubanska, J. Kucinska-Lipka, H. Janik, *Polymers* **2018**, *10*, 1304.
[19] S. H. Keshel, S. N. K. Azhdadi, A. Asefnejad, M. Sadraeian, M. Montazeri, E. Biazar, *Int. J. Nanomed.* **2011**, *6*, 641.
[20] H. Makki, K. N. S. Adema, M. M. R. M. Hendrix, E. A. J. F. Peters, J. Laven, L. G. J. Van Der Ven, R. A. T. M. Van Benthem, G. De With, *Polym. Degrad. Stab.* **2015**, *122*, 180.
[21] M. Gircys, B. J. Ross, *Complexity* **2019**, *2019*, 7293193.
[22] M. Dominici, K. Le Blanc, I. Mueller, I. Slaper-Cortenbach, F. C Marini, D. S. Krause, R. J. Deans, A. Keating, D. J. Prockop, E. M. Horwitz, *Cytotherapy* **2006**, *8*, 315.
[23] S. Pina, R. F. Canadas, G. Jimenez, M. Perán, J. A. Marchal, R. L. Reis, J. M. Oliveira, *Cells Tissues Organs* **2017**, *204*, 150.
[24] K.-C. Hung, C.-S. Tseng, S.-H. Hsu, *Adv. Healthcare Mater.* **2014**, *3*, 1578.
[25] C. Wang, N. Feng, F. Chang, J. Wang, B. Yuan, Y. Cheng, H. Liu, J. Yu, J. Zou, J. Ding, X. Chen, *Adv. Healthcare Mater.* **2019**, *8*, 1970056.
[26] J. W. Lee, G. Ahn, J. Y. Kim, D.-W. Cho, *J. Mater. Sci.: Mater. Med.* **2010**, *21*, 3195.
[27] R. A. Perez, G. Mestres, *Mater. Sci. Eng., C* **2016**, *61*, 922.
[28] Se H Oh, T. Ho Kim, G. Il Im, J. Ho Lee, *Biomacromolecules* **2010**, *11*, 1948.
[29] D. Martínez-Moreno, G. Jimenez, C. Chocarro-Wrona, E. Carrillo, E. Montanez, B. Clares-Naveros, G. Rus, J. De Vicente, J. A. Marchal, *Mater. Sci. Eng., C* **2021**, *122*, 111933.
[30] K.-C. Hung, C.-S. Tseng, L.-G. Dai, S.-H. Hsu, *Biomaterials* **2016**, *83*, 156.
[31] G. T. Howard, *Int. Biodeterior. Biodegrad.* **2002**, *49*, 245.
[32] J. P. Dahl, M. Caballero, A. K. Pappa, G. Madan, W. W. Shockley, J. A. Van Aalst, *Otolaryngol.–Head Neck Surg.* **2011**, *145*, 915.
[33] Y.-T. Wen, N.-T. Dai, S.-H. Hsu, *Acta Biomater.* **2019**, *88*, 301.
[34] B. Kundu, M. Eltohamy, V. K. Yadavalli, S. C. Kundu, H.-W. Kim, *ACS Appl. Mater. Interfaces* **2016**, *8*, 28458.
[35] Y.-C. Kuo, R. Rajesh, *Mater. Sci. Eng., C* **2017**, *77*, 680.
[36] T. Dvir, B. P. Timko, D. S. Kohane, R. Langer, *Nat. Nanotechnol.* **2011**, *6*, 13.
[37] J. Li, X. Mou, J. Qiu, S. Wang, D. Wang, D. Sun, W. Guo, D. Li, A. Kumar, X. Yang, A. Li, H. Liu, *Adv. Healthcare Mater.* **2015**, *4*, 998.
[38] Y. N. Sergeeva, T. Huang, O. Felix, L. Jung, P. Tropel, S. Viville, G. Decher, *Biointerphases* **2016**, *11*, 019009.
[39] N. Kohli, V. Sharma, S. J. Brown, E. García-Gareta, *Biomaterials for Skin Repair and Regeneration*, 1st, Woodhead Publishing **2019**, pp. 125–149, https://www.sciencedirect.com/science/article/pii/B9780081025468000054?via%3Dihub
[40] C. Chocarro-Wrona, J. Vicente, C. Antich, G. Martínez-Moreno, E. Carrillo, E. Montañez, J. A. Marchal, *Bioeng. Transl. Med.* **2021**, *6*, e10192.
[41] W. Dai, N. Kawazoe, X. Lin, J. Dong, G. Chen, *Biomaterials* **2010**, *31*, 2141.
[42] P. Singh, J. E. Schwarzbauer, *J. Cell Sci.* **2012**, *125*, 3703.
[43] R. Cai, T. Nakamoto, N. Kawazoe, G. Chen, *Biomaterials* **2015**, *52*, 199.
[44] G. Luo, J. Wang, Y. Wang, B. Feng, J. Weng, *J. Microencapsulation* **2015**, *32*, 129.
[45] M. Santin, A. Motta, S. P. Denyer, M. Cannas, *Biomaterials* **1999**, *20*, 1245.
[46] I. Sallent, H. Ctor Capella-Monsonís, D. I. Zeugolis, https://doi.org/10.1007/978-1-4939-9095-5_3 (accessed: August 2021).
[47] W. Wan, Y. Lin, A. Prakash, Y. Zhou, *J. Mater. Chem. A* **2016**, *4*, 18687.
[48] P. H. Byers, J. F. Bonadio, in *Genetic and Metabolic Disease in Pediatrics: Butterworths International* (Eds: J. K. Lloyd, C. R. Scriver), Butterworth-Heinemann, **2014**, pp. 56.
[49] S. Dietze, W. Yan, Y. Liu, L. Fang, K. Kratz, A. Lendlein, F. Jung, *Clin. Hemorheol. Microcirc.* **2018**, *70*, 511.
[50] C. Antich, J. Vicente, C. Chocarro-Wrona, E. Carrillo, J. A. Marchal, *Adv. Healthcare Mater.* **2021**, *10*, 2001847.
[51] S. Ghosh, M. Laha, S. Mondal, S. Sengupta, D. L. Kaplan, *Biomaterials* **2009**, *30*, 6530.

[52] T. Masutani, S. Yamada, A. Hara, T. Takahashi, P. G. Green, M. Niwa, *Int. J. Mol. Sci.* **2020**, *21*, 7744.
[53] J. Lu, X. Shen, X. Sun, H. Yin, S. Yang, C. Lu, Yu Wang, Y. Liu, Y. Huang, Z. Yang, X. Dong, C. Wang, Q. Guo, L. Zhao, X. Sun, S. Lu, A. G. Mikos, J. Peng, X. Wang, *Theranostics* **2018**, *8*, 5039.
[54] Y. Zhang, X. Liu, L. Zeng, J. Zhang, J. Zuo, J. Zou, J. Ding, X. Chen, *Adv. Funct. Mater.* **2019**, *29*, 1970246.
[55] M. Kouhi, M. Fathi, M. P. Prabhakaran, M. Shamanian, S. Ramakrishna, *Mater. Today: Proc.* **2018**, *5*, 15702.
[56] Z. Wang, H. Le, Y. Wang, He Liu, Z. Li, X. Yang, C. Wang, J. Ding, X. Chen, *Bioact. Mater.* **2022**, *11*, 317.
[57] D. Martínez-Moreno, G. Rus, J. A. Marchal, *Biochim. Biophys. Acta, Mol. Basis Dis.* **2019**, *1865*, 1067.
[58] E. L. Radin, D. B. Burr, B. Caterson, D. Fyhrie, T. D. Brown, R. D. Boyd, *Semin. Arthritis Rheum.* **1991**, *21*, 12.
[59] D. He, H. Li, *J. Mater. Sci. Technol.* **2021**, *63*, 62.
[60] H. Muhammad, Y. Rais, N. Miosge, E. M. Ornan, *Cell. Mol. Life Sci.* **2012**, *69*, 2101.
[61] C. E. Farnum, N. J. Wilsman, *Anat. Rec.* **2011**, *294*, 533.
[62] D. R. Rich, A. L. Clark, *Osteoarthritis Cartilage* **2012**, *20*, 923.
[63] N. S Stott, T.-X. Jiang, C.-M. Chuong, *J. Cell. Physiol.* **1999**, *180*, 314.
[64] F. Accadbled, T. T. Pham, C. Thevenin Lemoine, *Am. J. Case Rep.* **2020**, *21*, e920688.
[65] E. López-Ruiz, M. Perán, J. Cobo-Molinos, G. Jiménez, M. Picón, M. Bustamante, F. Arrebola, M. C. Hernández-Lamas, A. D. Delgado-Martínez, E. Montañez, J. A. Marchal, *Osteoarthritis Cartilage* **2013**, *21*, 246.
[66] F. Galisteo-González, J. A. Molina-Bolívar, S. A. Navarro, H. Boulaiz, A. Aguilera-Garrido, A. Ramírez, J. A. Marchal, *Colloids Surf., B* **2018**, *165*, 103.
[67] K. Chabi Sika, T. Kefela, H. Adoukonou-Sagbadja, L. Ahoton, A. Saidou, L. Baba-Moussa, L. Jno Baptiste, S. O. Kotconi, E. W. Gachomo, *Plant Gene* **2015**, *1*, 43.
[68] E. Lopez-Ruiz, G. Jimenez, W. Kwiatkowski, E. Montanez, F. Arrebola, E. Carrillo, S. Choe, Ja Marchal, M. Perãn, *Eur. Cells Mater.* **2018**, *35*, 209.